Electronic Supplementary Material (ESI) for Lab on a Chip.

Supplementary information for:

Holographic flow scanning cytometry overcomes depth of focus limits and smartly adapts to microfluidic speed

1. Taking conventional DH as ground truth to evaluate the reconstruction results of ASTDH

Phase-contrast imaging of cells based on conventional DH is a mature and well-developed technology, it allows quantitative phase evaluation of cells without staining [S1-3]. Considering that STDH has the same recording geometry as a conventional off-axis DH, the ground truth for STDH phase result is the phase information estimated by conventional DH.

In the related experiment of proposed manuscript, an area array CCD camera was used to record conventional off-axis holograms. This creates the possibility for comparing side-by-side ASTDH results with conventional DH results under the same conditions. Essentially, the use of area array camera is not a sound strategy for STDH, while using a line scan camera is a key concept and advantage of the proposed approach; however, in order to benchmark ASTDH using conventional DH as a reference, in this set of experiments we used an area array camera instead of a linear sensor array at the cost of recording speed.

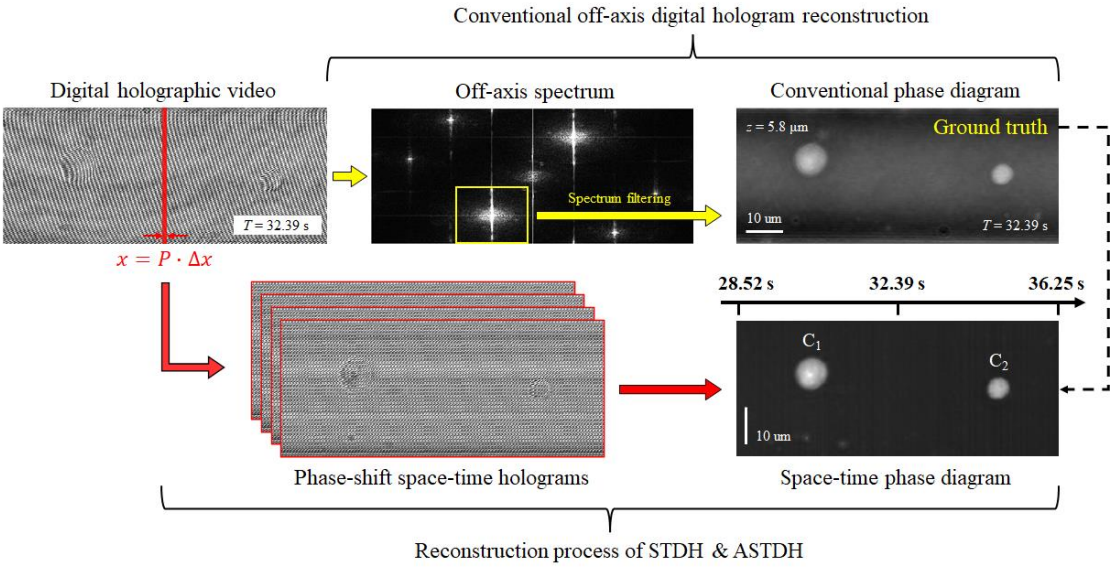

Figure S1. Reconstruction routes of conventional DH and ASTDH based on off-axis holograms

The illustration in Figure S1 shows the differences between the main processing steps of DH (ground-truth) and ASTDH reconstructions that lead to phase-contrast estimation. Conventional off-axis DH reconstruction is based on a demodulation process carried out through Fourier spectrum filtering. The -1 order and 0 order are filtered out before zero-padding and the +1 order is selected and demodulated. After this, numerical diffraction propagation and phase unwrapping are performed to obtain the phase information of the object. In most cases, a phase de-distortion

process is required to further suppress the background noise. At the top-right corner in Figure S1, we show a phase map of two selected cells (C_1 and C_2 in Figure 4 of main text), reconstructed by conventional DH. The selected frame is the hologram at time T = 32.39 s; it is propagated to the plane at z = 5.8 μm. Then, in bottom line of Figure S1, the common approach of STDH and the novel ASTDH is shown. Instead of reconstructing the full hologram directly, it extracts the columns with $P \cdot \Delta x$ pixels and reassemble them in chronological order to form a space-time hologram. Phase-shift processing is performed to obtain the object complex amplitude. This is different from spectrum filtering of conventional off-axis DH and in general it allows to preserve better the high frequency content of the hologram (it avoids Fourier filtering). Comparing the reconstruction results obtained by the two different methods, they maintain a good consistency in shape and relative position.

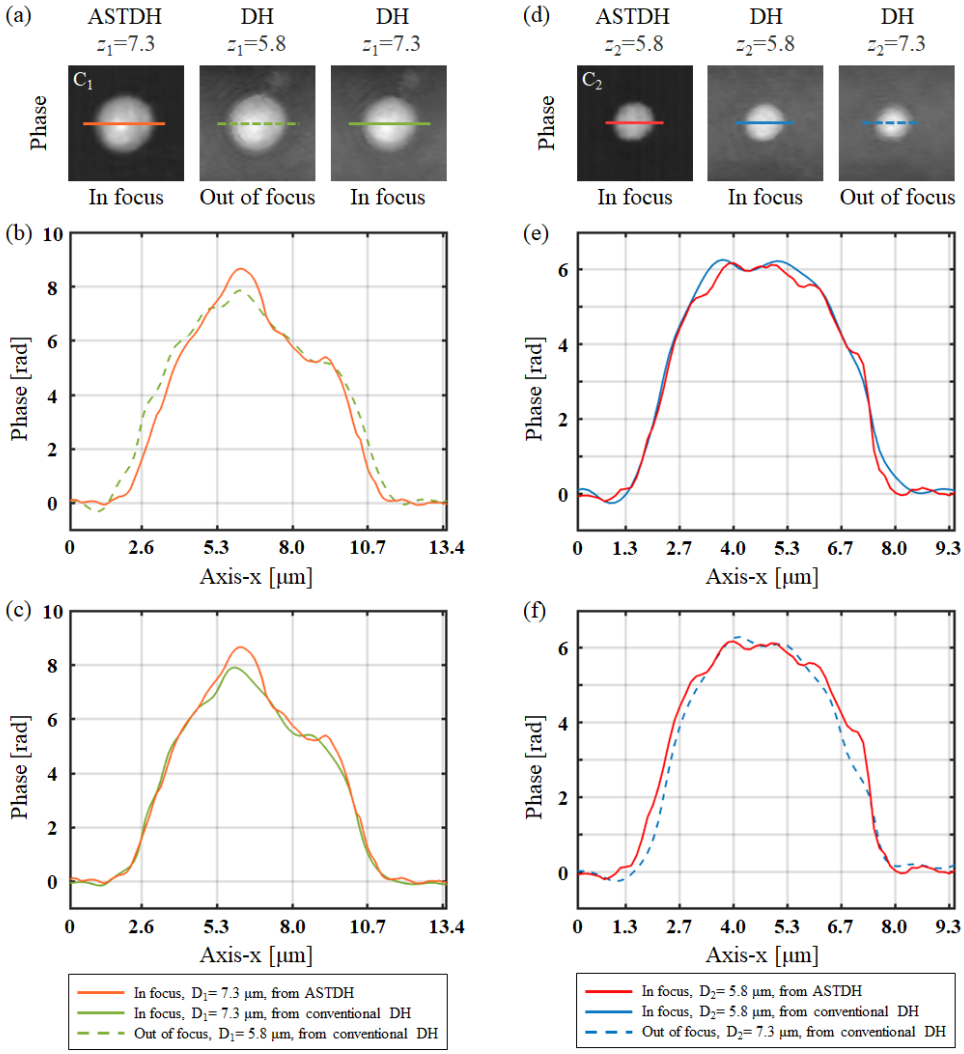

Figure S2. Comparison of cells C_1 and C_2 under two different reconstruction methods. (a) Phase maps of cell C_1 under ASTDH and conventional DH, it focuses on the plane of 7.3 μm. (c) and (b) are the sectional views of (a). The orange solid lines indicate the focused cell phase of ASTDH; the green solid line indicates the focused cell phase of DH; the green dotted line indicates the out of focus cell phase. (d) Phase maps of cell C_2 under ASTDH and conventional DH, it focuses on the plane of 5.8 μm. (e) and (f) are the sectional views of (d). The red solid lines indicate the focused cell phase of ASTDH; the blue solid line indicates the focused cell phase of DH; the blue dotted line indicates the out of focus cell phase.

To better compare the reconstruction results between conventional off-axis DH and ASTDH for the same holograms, we plotted the sectional images of cells C_1 and C_2 under the two reconstruction methods. Herein, ASTDH applied a multi-level focusing strategy based on strip reconstruction, so both C_1 and C_2 are in focus. Conventional DH results require an overall reconstruction of the hologram to preserve resolution, so two phase results at different reconstruction distances are chosen, which are 5.8 μm and 7.3 μm. For the cell C_1, it is in the plane of 7.3 μm of MFC. Therefore, C_1 cannot be accurately focused on the 5.8 μm plane where C_2 is focused. When comparing the plots of the cell in plane 5.8 μm, it can be seen that the DH phase curve of C_1 is less sharp than that of the focused ASTDH phase curve in Figure S2(b). When the reconstruction planes of the two methods are in plane 7.3 μm, the two curves have a good agreement. This also means that ASTDH reconstruction maintains the same cell's size as the conventional DH reconstruction. It is worth mentioning that ASTDH has obtained a significant contrast improvement in the internal information of the cell, which can be clearly observed from the comparison of the curves in Figure S2(c). A similar contrast enhancement can be observed in the comparison of cell C_2 in Figure S2(e). While both methods ensure that C_2 is in focus, the ASTDH method clearly reveals phase changes in cellular regions. The principle of contrast and resolution improvement based on STDH strategies has been demonstrated in our previous studies, please refer to Reference 36 in main text.

By analyzing the results of the above curves, once the cells C_1 and C_2 are all in the focal plane, the results obtained by the two methods are in good agreement. The multi-level focusing ability of ASTDH successfully focuses two cells, which are on different planes, to the same reconstruction plane. This effectively avoids multiple propagations of the complete hologram in the conventional DH reconstruction process. Moreover, ASTDH can achieve higher phase-contrast then conventional DH, which would allow performing more precise analysis and cell classification.

For further comparison between conventional DH and ASTDH based on same data sets, the holograms, which contain the cells zoomed in in Figure 6, are reconstructed by conventional off-axis DH, as shown in Figure S3.

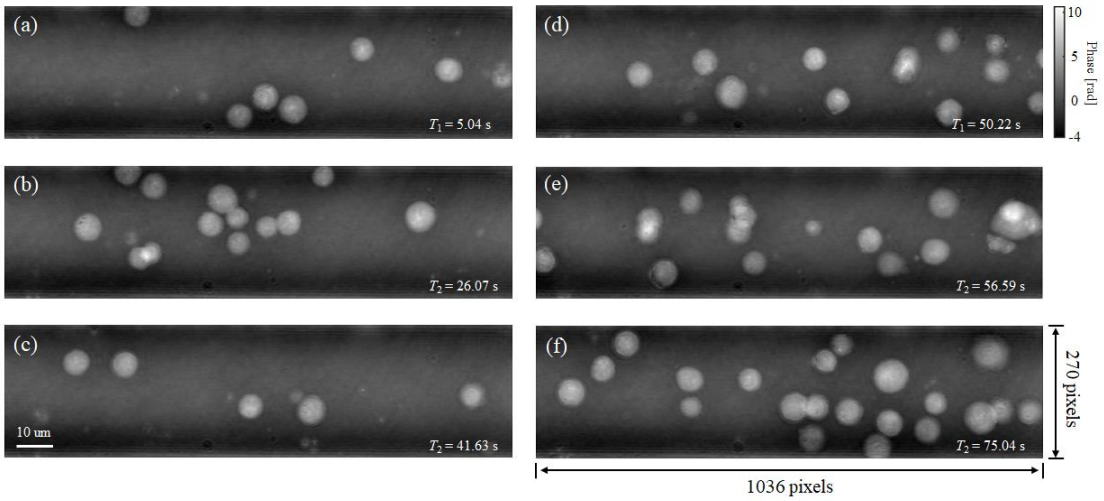

Figure S3. Phase maps of selected cells based on conventional DH. (a)-(f) results of six time points, each of them contains the same cells zoomed-in in Figure 6.

Compared to conventional DH cell imaging, which is deeply assessed as a metrology tool, ASTDH has four advantages. Firstly, with the same information content, ASTDH requires less storage space compared with conventional DH. A single conventional hologram only contains the 3D spatial distribution of cells at a certain moment, and does not contain velocity information, so it is necessary to store a time-series of holograms. ASTDH

intrinsically encodes the time distribution of cells flowing in the channel during the experiment. Secondly, conventional off-axis reconstruction is difficult to deal with the background information of microfluidic channels, especially the phase fluctuation caused by the change of flow velocity. As shown in Figure S3, all phase maps exhibit non-flat background, despite previous phase calibration processes. In the case of ASTDH, background noise removal is trivial because it uses a fixed position for space-time hologram encoding. Thirdly, the reconstruction of ASTDH is based on a phase shifting process. Compared with spectrum filtering in conventional off-axis reconstruction, it can preserve better high-frequency information from the same hologram. Above all, STDH allows the use of high-speed line scanning cameras, which is impossible for conventional off-axis geometry. Meanwhile, the strip-based reconstruction process creates the possibility for fast multi-point focusing of cells. The results in Figure S3 show the limitations of conventional off-axis DH, compared to ASTDH, since the cells are not in focus simultaneously and do not have flow information in a single frame. Therefore, ASTDH takes less time and computing resources to reconstruct the same information than conventional DH.

2. Estimating the correction α factor by standard deviation optimization

In the proposed ASTDH strategy, the α factor acts on the numerical propagation process, but the optimization of the α factor and the focusing process of the sample itself are performed separately. The cell is propagated to its best-focus plane firstly, then the α factor is optimized. This means that all cells are in-focus before calculating the standard deviation as a function of α. The sub-pixels mismatch results in the appearance of additive banding noise (see e.g. top of Fig. S4). Suppressing this noise term is the main role of α factor. The sub-pixel mismatch refers to the sub-pixel difference between the two members of the matching condition. If the matching condition is not satisfied in full, there is a discrepancy between the synthetic object representation by STDH and the ground truth.

The sub-pixel mismatch causes missing information at the sampling point (local undersampling of the space-time hologram in correspondence to the locations where the matching condition is not met), which shows as banded diffraction noise in the imaging plane.

The banding noise is displaced normally to the scan direction and adds an unwanted modulation to the phase of the cell. By introducing the α factor in the numerical propagation kernel, this effect can be reduced, resulting in a reduction in the standard deviation of the overall phase values. For this reason, we chose to minimize the phase standard deviation to estimate the best α factor. As shown in Figure S4, comparisons with the conventional DH acquisitions for the same cells demonstrates that this process can remove the modulation effect and restore the original phase distribution of the cells.

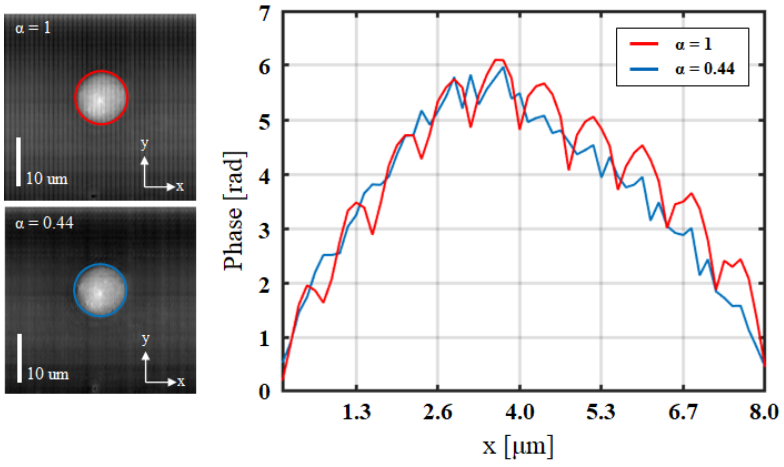

Figure S4. Cell phase distribution at the focal plane under different α factors. The curves reveal the distribution of

cell areas averaged along the y direction.

Figure S4 shows the cell phase distribution under different α-factors for a cell in focus. The propagation distance required for the cells to focus on the imaging plane is calculated firstly, then two different α factors are implemented during numerical propagation. After the cell area is determined by the edge extraction algorithm, the phase sectional view is obtained by taking the average along the y-axis direction only in the cell area. The results clearly show banding noise due to subpixel mismatch, and this noise is minimized at $\alpha = 0.44$, which corresponds to a minimum of the phase standard deviation as a function of α.

3. Evaluation of the minimum propagation window during stripe-based numerical reconstruction

Strip reconstruction is an optimization of the conventional digital holographic reconstruction process in the STDH paradigm. It is implemented to reduce the calculus time and create the possibility of parallel processing by reducing the working window size along the scanning direction. However, reducing too much the window size corresponds to reducing the numerical aperture of the system, thus introducing a resolution loss. In general, the minimum size for the working window that allows maintaining lateral resolution varies with the optical setup parameters. For the actual 34× magnification and 4.54×4.54 μm^2 camera pixel size, the minimum allowed size along scanning direction is 201 pixels. This value was experimentally measured, using the STDH image of a USAF-1951 resolution target, which let us determining the minimum strip width that allows reducing computational times while avoiding resolution losses. The results of this preliminary estimation process are shown in Figure S5.

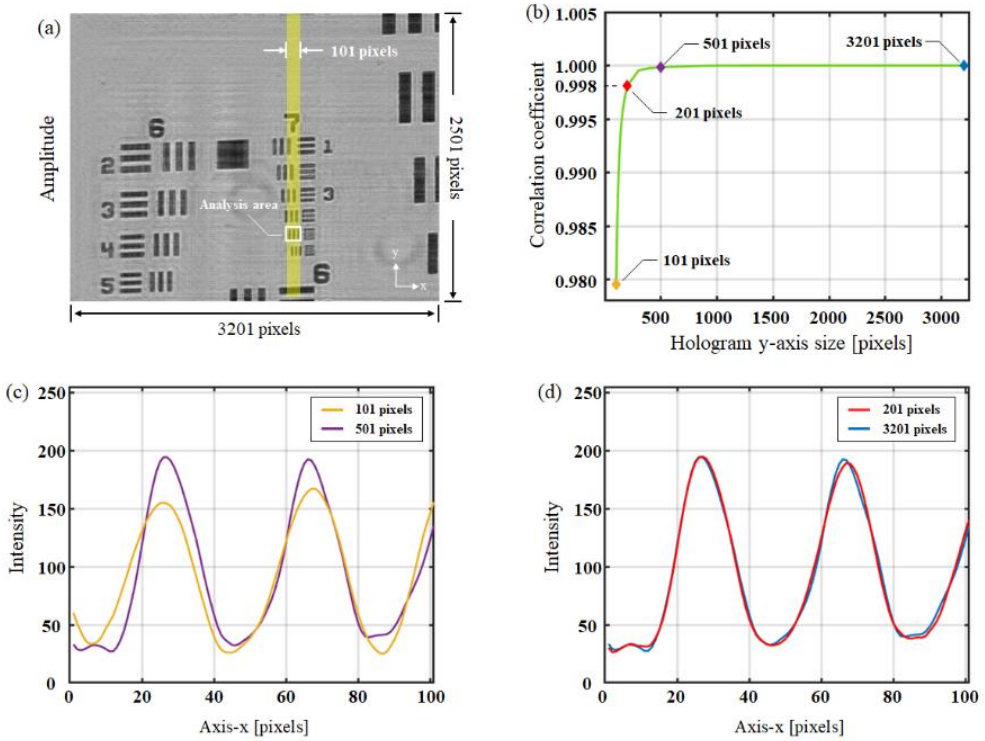

Figure S5. Estimating the minimum strip width from STDH of USAF-1951 resolution target. (a) USAF-1951 amplitude map obtained based on STDH recording and reconstruction; the yellow highlighted area shows the zone of the correlation calculation. (b) Correlation coefficient curves of results extracted from different strip widths with full field. (c) and (d) are the curves of sectional views for the average along the y-axis of white solid line frame area in (a).

The target was moved by an electronically controlled 1D linear stage; according to the frame rate 13.5 FPS of camera, the moving velocity of target was set to 1.80 μm/s. This would allow the synthesis and phase-shift reconstruction of conventional space-time holograms. Figure S5(a) shows the full field reconstructed amplitude result of the target. A working window, which is 3201×2501 pixels, including 6th and 7th line pairs was selected for further analysis, as shown in Figure S5(a). In order to evaluate the information loss during the process of numerical propagation with different strip widths, we crop the full-field space-time hologram into strips of different sizes, from 101 to 3201 pixels in scanning direction, and propagated the strips. The 101×2501 pixels object section highlighted in yellow in Fig. S5(a), obtained from full-field reconstruction is set as a ground truth. The propagated strips of different widths are compared with the ground truth by correlation coefficient measurement after cropping the same FoV. Fig. S5(b) shows the curve of correlation coefficients as a function of the strip width. From 101 to 501 pixels, the correlation coefficient keeps increasing. After reaching 501 pixels, the correlation coefficient is 1, which means the reconstructed amplitude is fully consistent with the ground truth. The correlation coefficient reaches 0.998 at 201 pixels. Further width increases only determine a negligible increase of the correlation coefficient, so that the value 201 has been set as an optimal trade-off between accuracy and computational cost. The curves of sectional views in Figures S5 (c) and (d) also support this conclusion.

For the above-mentioned reasons, during the reconstruction process of proposed ASTDH method, the size of propagation window along scanning direction is set to 201 pixels.

4. Effect of the *P* factor for preliminary calibration of squeezed cells.

In the experimental results we have shown in Figure 6, a good example to reveal the role of the *P* factor is the set of cells from 3.46s to 9.63s. As shown in Figure S6(a), when $P = 5$ was applied to all five cells, unwanted squeezing occurred for the two cells in the upper right corner. This is due to undersampling caused by a mismatch between the cell flow rate and the equivalent pixel in the image plane, which is not properly corrected due to an incorrect choice for the *P* factor. For the cells with velocity 9.6 ± 1.0 μm/s, setting the sampling factor $P_{1-3} = 5$ can ensure that the cell size is consistent with the ground truth from conventional DH. But for cells with a flow rate higher than this value, the *P* factor needs to take a larger value to ensure well-sampling. For the results shown in Figure S6(b), cell No.4 and cell No.5 need different *P* factors, i.e. $P_4 = 8$ and $P_5 = 7$. In this case, all five cells meet the ground truth. After calculation, the velocity of Cell No.4 is 15.3 ± 1.0 μm/s and Cell No.5 is 13.4 ± 1.0 μm/s. The results described above intuitively illustrate the role of the P factor in ASTDH reconstruction.

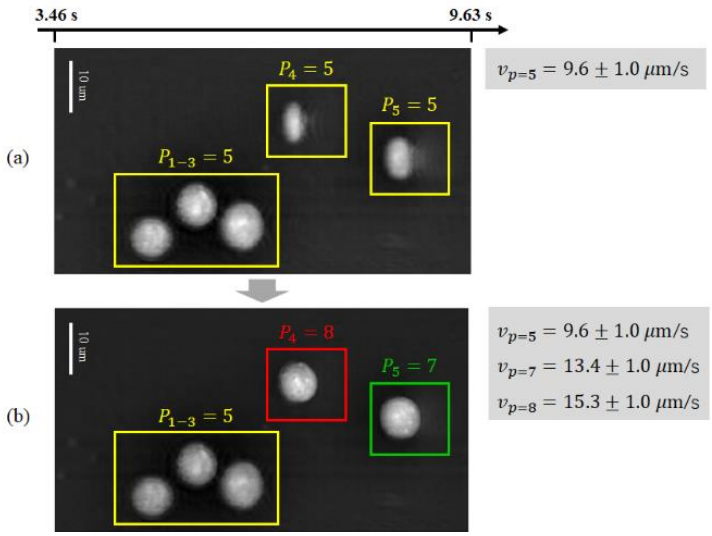

Figure S6. Reconstruction results of tuning the assembly process based on the *P* factor. (a) Using the same *P* factor

to assemble and reconstruct space-time holograms. (b) Adjusting the *P* factor according to cell flow rate and performing reconstruction.

5. Computing cost and hardware information

The computational time required to obtain the results in Figure 6 can be divided into two parts: assembling of space-time hologram and phase information reconstruction. For a space-time hologram with 7200×271 pixels, the hologram assembly and phase shifting process took 721.34 s using a conventional laptop; the phase information extraction (including multi-cell focusing) took 242.26 s. None of them used parallel computing. In this case, to reconstruct the phase images in Figure 6 from recorded holographic video, the total time cost is 963.60 s. For the same sequence, consisting of 1200 holograms, conventional DH processing would take about 9450 s using the same hardware. In other words, more than a nine-fold factor of improvement in terms of computational time can be obtained by ASTDH due the large data compression it allows. The hardware of laptop for computation is CPU Intel i5-8365U 1.60GHz, RAM 8G, without discrete graphics card.

References

[S1] Javidi, Bahram, et al. "Roadmap on digital holography." Optics Express 29.22 (2021): 35078-35118.

[S2] Langehanenberg, Patrik, et al. "Autofocusing in digital holographic phase contrast microscopy on pure phase objects for live cell imaging." Applied optics 47.19 (2008): D176-D182.

[S3] Kim, Myung K. "Digital holographic microscopy." Digital Holographic Microscopy. Springer, New York, NY, 2011. 149-190.